Two-step excitation and direct two-photon absorption in Tb3+:LiYF4
by Richard Paul Jones

A thesis submitted in partial fulfillment of the requirements for the degree of Master of Science in Physics
Montana State University

Abstract:
Two-photon absorption is used to study highly excited levels of the Tb3+ ion. The known energy levels of Tb3+ have thus been extended to much higher energies. This work also makes contributions to the study of these highly excited levels through accurately measured energies and discriminations between those levels which are intrinsic and those which are due to crystal defects.

These experiments involved using either one or two pulsed tunable dye lasers operating in the visible range of the spectrum. The levels studied included the 5K9, 5D2, 5G6, 5K8, a second 5G6, 5K5, and 5K7 of the 4f8 configuration of Tb3+ in a host crystal of LiYF4. These levels correspond to a total studied energy range of 39,100 cm-1 to 42,000 cm-1.

These experimentally measured energies are compared with an advanced computer-fitted free ion and crystal field model showing a high degree of correlation between experiment and theory. The population of these highly excited states was sensitively monitored by observing the anti-Stokes ultraviolet cascade fluorescence from 5D3 to 7F5. Energy levels due to crystal defects were discriminated against the intrinsic energy levels by controlling the laser timing in the two-laser two-step excitation experiments.

These results suggest that the selection rules for pure 4f8 configurations as applied to direct two-photon absorption are not entirely valid and can be broken. This provides further support for a theory of resonant enhancement.

TWO-STEP EXCITATION AND DIRECT TWO-PHOTON ABSORPTION IN Tb^{3+}:$LiYF_4$

by

Raymond Paul Jones

A thesis submitted in partial fulfillment
of the requirements for the degree

of

Master of Science

in

Physics

MONTANA STATE UNIVERSITY
Bozeman, Montana

June 1990

APPROVAL

of a thesis submited by

Raymond Paul Jones

This thesis has been read by each member of the thesis committee and has been found to be satisfactory regarding content, English usage, format, citations, bibliographic style, and consistency, and is ready for submission to the College of Graduate Studies.

May 14, 1990
Date

Rufus L Cone
Chairperson, Graduate Committee

Approved for the Major Department

May 14, 1990
Date

Head, Major Department

Approved for the College of Graduate Studies

June 5, 1990
Date

Henry L Parsons
Graduate Dean

STATEMENT OF PERMISSION TO USE

In presenting this thesis in partial fulfillment of the requirements for a master's degree at Montana State University, I agree that the Library shall make it available to borrowers under rules of the library. Brief quotations from this thesis are allowable without special permission, provided that accurate acknowledgement of source is made.

Permission for extensive quotation from or reproduction of this thesis may be granted by my major professor, or in his absence, by the Dean of Libraries when, in the opinion of either, the proposed use of the material is for scholarly purposes. Any copying or use of the material in this thesis for financial gain shall not be allowed without my written permission.

Signature 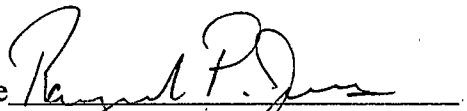

Date May 14, 1990

ACKNOWLEDGMENTS

The author would like to acknowledge and thank all those who assisted him in his graduate career at Montana State University. First and foremost is his advisor, Professor R.L. Cone, for providing the opportunity for conducting the research on which this thesis is based.

The author would also like to thank all those in the Physics Department who lended him support through discussions and assistance, especially Jin Huang and Liu Guokui for their assistance with the experimental apparatus. Thanks are due to Alfred Beldring for his knowledge and expertise in electronics and to Mark E. Baldwin for supplying liquid nitrogen in these experiments.

The author would like to thank the Physics Department at Montana State University and MONTS for financial assistance throughout this work.

Finally, the author would like to express his gratitude to his wife and family for all of their encouragement and assistance.

TABLE OF CONTENTS

TABLE OF CONTENTS — Continued

LIST OF TABLES

LIST OF FIGURES

LIST OF FIGURES — Continued

ABSTRACT

Two-photon absorption is used to study highly excited levels of the Tb^{3+} ion. The known energy levels of Tb^{3+} have thus been extended to much higher energies. This work also makes contributions to the study of these highly excited levels through accurately measured energies and discriminations between those levels which are intrinsic and those which are due to crystal defects.

These experiments involved using either one or two pulsed tunable dye lasers operating in the visible range of the spectrum. The levels studied included the $^5K_9$, $^5D_2$, $^5G_6$, $^5K_8$, a second $^5G_6$, $^5K_5$, and $^5K_7$ of the $4f^8$ configuration of Tb^{3+} in a host crystal of $LiYF_4$. These levels correspond to a total studied energy range of 39,100 cm^{-1} to 42,000 cm^{-1}.

These experimentally measured energies are compared with an advanced computer-fitted free ion and crystal field model showing a high degree of correlation between experiment and theory. The population of these highly excited states was sensitively monitored by observing the anti-Stokes ultraviolet cascade fluorescence from $^5D_3$ to $^7F_5$. Energy levels due to crystal defects were discriminated against the intrinsic energy levels by controlling the laser timing in the two-laser two-step excitation experiments.

These results suggest that the selection rules for pure $4f^8$ configurations as applied to direct two-photon absorption are not entirely valid and can be broken. This provides further support for a theory of resonant enhancement.

CHAPTER 1

INTRODUCTION

This thesis contributes to the study of the highly excited states of the Tb^{3+} ion through accurately measured energies and discriminations between those levels which are intrinsic and those which are due to crystal defects. The object of this study is to present new experimental energies for trivalent Terbium in a host crystal of $LiYF_4$. This work is particularly interesting in the fact that prior to it, the Tb^{3+} ion was essentially unstudied in any crystal over these energy ranges.

The absorption and emission spectra of rare earth ions in ionic crystals are particularly interesting since the optical linewidths can be as narrow as those in gases. This suggests that these rare earth ions are behaving as if they were almost free ions. In fact, this is somewhat true and is due to a shielding of the 4f electrons (where these transitions take place) by the outer 5s and 5p electrons. The deviations from this free ion model can then be accounted for by applying perturbations to the free ion Hamiltonian and rediagonalizing to obtain the new energies. This is not as easy as it sounds. The end result is that the calculated energy levels are written in terms of parameters that must be determined by comparison with experimentally measured energy levels.

Two non-linear optical processes were utilized to complete this task, these being Two-Step Excitation (TSE) and Direct Two-Photon Absorption (TPA). In a

TSE process, an atom is excited from its ground state to a real intermediate state by absorbing a single photon and then is excited again to a final state by the absorption of another photon of different energy. In a TPA process the atom is excited from the ground state to the final excited state by the simultaneous absorption of two photons having the same energy. Both of these processes will hereafter be referred to as two-photon transitions.

The advent of tunable dye lasers enabled researchers to observe these sharp parity-allowed $4f^n \rightarrow 4f^n$ two-photon transitions with much more ease. Prior to this development, the first two-photon transition was observed in Eu^{2+} in 1961 by Kaiser and Garrett, capitalizing on a broadband absorption feature that crystal has. [1] What is remarkable is that the basic theory of two-photon transitions was developed thirty years prior to this in 1931 by Göppert-Mayer. [2] In the time since Kaiser and Garrett's work however, considerable advances have been made in the field of two-photon transitions in rare earths, [3-9] as well as gases. [10]

Two-photon transitions have been previously observed in both dilute Tb^{3+}:$LiYF_4$ (1% concentration) and concentrated $LiTbF_4$ by Huang in 1987. [11] His experiments concentrated on the $^5G_6$ level of Tb^{3+}:$LiYF_4$ by both TPA and TSE and the $^5K_8$ level of $LiTbF_4$ by TSE. These present studies extend his work and are partially based upon work done by Cone at Bell Laboratories. [12] The Tb^{3+}:$LiYF_4$ crystal used is the same one used by Huang and Cone, and the energy levels studied were the $^5D_2$, $^5K_9$, $^5K_8$, a second order $^5G_6$ term, $^5K_5$, and $^5K_7$. Huang's results for the $^5G_6$ level with TPA were also reproduced in this work with a higher level of accuracy by using an opto-galvanic calibration system throughout the experiments. These levels correspond to a total studied energy range extending from 39,100 cm^{-1} to 42,000 cm^{-1}.

The selection rules (found through group theory considerations) for a single-

step excitation are different than those of a two-step excitation. In other words, each process by itself yields information that the other cannot. Therefore, when both process are considered together, a maximum amount of information is obtained, and the processes are said to be complementary. In a TPA process the selection rules allow for all possible transitions. This could lead one to believe that this is the ideal technique. However, the transition matrix element for a TPA process is a second order process in the atom-radiation interaction Hamiltonian, and thus its magnitude is very weak when compared to a single-step or two-step excitation. Certain other experimental difficulties, such as the dye laser broadband fluorescence and vibronic absorption, limited the use of TPA processes to only a few levels with the present experimental apparatus. These two-photon processes allowed for the study of energy levels up to 42,000 cm^{-1} with visible light, whereas one would need to use UV spectroscopy to study these same levels with single-step excitations. For these reasons outlined above, TSE was the primary means of obtaining information on these levels.

In this thesis, a brief description of the theory of two-photon transitions as well as a discussion of the selection rules applied to Tb^{3+}:$LiYF_4$ will be given in Chapter 2. This is followed by a description of the experimental apparatus and procedures in Chapter 3. A discussion of the experimental results will be given in Chapter 4 followed by some concluding remarks in Chapter 5.

CHAPTER 2

THEORY

The theory of two-photon absorption can be explained by several methods. One method involves expanding the macroscopic polarization in a power series of the optical electric field and taking the imaginary part of the third order nonlinear susceptibility. An alternate method is to treat the optical radiation field as a perturbation to the ionic Hamiltonian and to expand it to second order. Both of these methods are very well developed, so only a brief outline of the perturbation theory approach will be given.

The following derivation of the two-photon transition rate closely follows Gold, [13] so the reader can consult his work or any of the other references for further details. [14,15] Following the derivation, a brief description of the energy levels for Tb^{3+} will be given along with an explanation of the group theory approach to the selection rules.

Two-Photon Absorption

Consider a multi-level atomic system with definite eigenstates corresponding to the unperturbed hamiltonian,

$$H_0 \mid \Psi_n(r,t) \rangle = E_n \mid \Psi_n(r,t) \rangle, \tag{2.1}$$

where

$$\mid \Psi_n(r,t) \rangle = \mid \varphi_n(r) \rangle \exp(-i\Omega_n t). \tag{2.2}$$

The two-photon transition process will bring the system to a final excited state $|\Psi_f\rangle$ lying at an energy $E_{fg} = \hbar(\Omega_f - \Omega_g) = \hbar\Omega_{fg}$ above the ground state $|\Psi_g\rangle$. At $t = 0$ a perturbation H' is added so that the new hamiltonian is

$$H = H_0 + \lambda H', \tag{2.3}$$

where H' is an electric dipole interaction described by

$$H' = -er\cdot[E_1\varepsilon_1\exp(-i\Omega_1 t) + E_2\varepsilon_2\exp(-i\Omega_2 t)]. \tag{2.4}$$

The vectors ε_1 and ε_2 refer to the polarizations of the two respective electric fields E_1 and E_2, and Ω_1 and Ω_2 are the respective frequencies. At $t > 0$ there will be a superposition of the original eigenstates

$$\Psi = \sum_n a_n(t)\,\Psi_n(r,t) \tag{2.5}$$

which must obey Schrödinger's time-dependent equation

$$i\hbar\frac{\partial}{\partial t}\Psi = (H_0+\lambda H')\Psi. \tag{2.6}$$

Upon inserting the superposition state (2.5) above into (2.6), taking the vector product with $\langle k|$, and expanding to second order, the probability density for the population of the final state is found to be

$$|a^{(2)}_f|^2 = \left|\frac{2e^2E_1E_2}{\hbar}\right|^2 |R_{fg}|^2 \frac{\sin^2[\,\tfrac{1}{2}(\Omega_{fg} - \Omega_1 - \Omega_2)t]}{(\Omega_{fg} - \Omega_1 - \Omega_2)^2} \tag{2.7}$$

where

$$R_{fg} = \sum_k \frac{\langle f|\varepsilon_1\cdot r|k\rangle\langle k|\varepsilon_2\cdot r|g\rangle}{\hbar(\Omega_{kg} - \Omega_2)} + \frac{\langle f|\varepsilon_2\cdot r|k\rangle\langle k|\varepsilon_1\cdot r|g\rangle}{\hbar(\Omega_{kg} - \Omega_1)} . \qquad (2.8)$$

In the event that t becomes sufficiently large, the function

$$\frac{\sin^2[\ \tfrac{1}{2}(\Omega_{fg} - \Omega_1 - \Omega_2)t]}{(\Omega_{fg} - \Omega_1 - \Omega_2)^2}$$

behaves as a delta function, resulting in a transition rate of

$$\frac{1}{\tau} = \frac{d}{dt}|a^{(2)}_f|^2 = \frac{2\pi}{\hbar^2} e^4|E_1|^2|E_2|^2|R_{fg}|^2\ \delta(\Omega_{fg} - \Omega_1 - \Omega_2). \qquad (2.9)$$

Here, all of the non-resonant terms have been eliminated by use of the rotating wave approximation. The R_{fg} term is the main item of interest in this last equation. Through it, a detailed investigation can be made by varying the polarization of the incident beams. Since the states $|k\rangle$ in equation 2.8 run over the complete set of eigenstates of the unperturbed hamiltonian H_0, the function

$$\sum_k \frac{|k\rangle\langle k|}{\hbar(\Omega_{kg} - \Omega_j)} \qquad (2.10)$$

transforms as an identity representation. This simplifies equation (2.8) and all of the relevant information can found from the matrix elements

$$\langle f|r_1 r_2|g\rangle, \qquad (2.11)$$

where r_1 and r_2 are the projections of ε_1 and ε_2 on r and

$$\mathbf{r} = \sum_i \mathbf{r}_i \qquad (2.12)$$

is the position operator of the electrons.

Energy Structure of Terbium

The electronic configuration of the terbium atom is that of xenon plus eleven more electrons. These start to fill the 4f and 6s shells resulting in an electronic configuration of

$[Xe]\ 4f^9\ 6s^2$.

When terbium is placed in a suitable host lattice and becomes triply ionized the two 6s electrons and one 4f electron are removed and its electronic configuration becomes

$[Xe]\ 4f^8$.

The 5s and 5p electrons are located spatially further from the nucleus and therefore serve to shield the 4f electrons from the outside environment. This sort of phenomenon gives all rare earths their gas-like spectral properties.

One now might think that there should be no visible allowed transitions since all the transitions will take place within the 4f shell, with no resulting change in the parity. However, configuration mixing due to the crystal field does allow these transitions to take place.

The energy levels are normally labeled in Russell-Saunders term notation. However, both the coulomb interaction and spin-orbit interaction are comparable in magnitude, and an intermediate coupling scheme needs to be applied. Due to the large number of particles with an orbital angular momentum of three in the Tb^{3+} ion, some S and L terms will occur more than once. New additional quantum

numbers need to be taken into account. J still continues to be a good quantum number.

Much work has been done on determining the lower energy levels of Tb^{3+} that will not be discussed in this thesis. [16-19] The references are cited for the interested reader.

Crystal Field

The host crystal for this particular set of experiments was $LiYF_4$ which crystallizes in a tetragonal scheelite structure. This crystal was doped with 1% Tb^{3+}, with the Tb^{3+} ions taking the place of Y^{3+} ions, resulting in each Tb^{3+} ion having an S_4 site symmetry. The S_4 symmetry operator is the basic element of the group, and it involves a rotation of $\pi/2$ about the symmetry axis followed by a reflection in a plane perpendicular to this axis of rotation. Since this operation does not alter the crystal structure in any way, it must commute with the crystal field hamiltonian.

The crystal field hamiltonian can be expressed as [16]

$$H_{cf} = \sum_{k=1}^{6} B_{kq} C_q^{(k)} \qquad (2.13)$$

where $C_q^{(k)}$ are spherical harmonics and B_{kq} are empirically determined parameters. The crystal field removes the spherical symmetry of the free ion, and hence, removes some of the 2J+1 degeneracy of the energy levels.

Group Theory

Since the crystal field hamiltonian and the S_4 symmetry operators commute they must have common eigenfunctions. Therefore, in determining the effect of the crystal field on the free ion hamiltonian one can utilize a group theory approach. A

brief outline of the application of this theory will be given here. For more of the specifics the reader can consult any of the references. [20-22]

The S_4 symmetry group is composed of four separate symmetry operations. These are E (the identity operation), C_2 (a rotation of π), S_4 (a rotation of $\pi/2$ followed by a reflection), and S_4^{-1} (the inverse of S_4). A multiplication table can then be constructed showing that any combination of these operations is identical to one of the four basic elements. Each of these symmetry operations can be mapped into four separate irreducible matrix representations Γ_1, Γ_2, Γ_3, and Γ_4, each of which will satisfy the multiplication table. These last two, Γ_3 and Γ_4, are actually complex conjugates of one another and are therefore degenerate. They will both be refered to as $\Gamma_{3,4}$.

The trace of each matrix in a particular representation is called its character (χ_{sk}) where s refers to a particular representation and k refers to a particular symmetry operation. A character table can then be written out as follows. [23]

Table 1. Character Table of the S_4 Group

	Character (χ_{sk})			
Γ_s	E	C_2	S_4	S_4^{-1}
Γ_1	+1	+1	+1	+1
Γ_2	+1	+1	−1	−1
Γ_3	+1	−1	−i	+i
Γ_4	+1	−1	+i	−i

The energy levels are characterized by the total angular momentum J, and therefore have a degeneracy of 2J+1. The effect of the crystal field is to remove

some of this degeneracy, making the previously irreducible representation (Γ_J) of a particular energy level reducible. The number of times each new irreducible representation (Γ_S) is contained in the reducible representation (Γ_J) is given by [20,21]

$$p_{SJ} = \frac{1}{n} \sum_{k=1}^{c} h_k \, \chi_J(\alpha_k) \, \chi_{Sk}^{*}. \qquad (2.14)$$

Here, n is the number of operations, h_k is the number of times an element occurs, c is the number of irreducible representations, and $\chi_J(\alpha_k)$ is the character of each operator for a particular reducible representation Γ_J with respect to the group of three dimensional rotations (R_3). These can be calculated from [20,21]

$$\chi_J(\alpha_k) = \frac{\sin (2J+1) \, \alpha/2}{\sin (\alpha/2)} \quad . \qquad (2.15)$$

Using equations (2.14) and (2.15) along with Table 1 gives the following table of crystal field splittings for the J multiplets.

Table 2. Crystal Field Splittings of J Multiplets

	Occurence of each Irreducible Representation		
J	Γ_1	Γ_2	$\Gamma_{3,4}$
0	1	0	0
1	1	0	1
2	1	2	1
3	1	2	2
4	3	2	2
5	3	2	3
6	3	4	3
7	3	4	4
8	5	4	4
9	5	4	5

Thus, it has been shown how a particular energy level would have some of its 2J+1 degeneracy removed by the crystal field. As an example, consider the $^7F_6$ ground state term of Tb^{3+}. Using table 2 above we can see that it would have 10 sublevels, 3 being of Γ_1, 4 being of Γ_2, and 3 being of $\Gamma_{3,4}$. This is represented with the expression $3\Gamma_1 + 4\Gamma_2 + 3\Gamma_{3,4}$.

Selection Rules

The primary mechanism for optical transitions is by electric dipole interactions. Magnetic dipole and electric quadrupole interactions are also allowed, but their relative magnitudes are far less than those of electric dipole transitions. Just as the energy eigenstates transform as certain representations, so do the electric and magnetic dipole operator vector components. The components needed for

determining the selection rules are x, y, and z for the electric dipole operator and L_x, L_y, and L_z for the magnetic dipole operator. The representations of these for a particular symmetry can be found in Tinkham's book. [20]

For a TSE process the transition is actually two single-photon transitions. Consequently, two applications of the single photon selection rules are necessary. Determining these selection rules involves operating on the initial (or intermediate) state with the electric dipole operator and looking at the resultant representation of this product. This can be done by using the group multiplication tables found in Koster's book. [23] Then, if the final state has the same representation as that of this product, the transition will be allowed. Table 3 can be constructed by applying this procedure to all representations.

Table 3. Selection Rules in S_4 Symmetry with Electric Dipole Transitions

	Polarization with respect to the crystal axis		
	Γ_1	Γ_2	$\Gamma_{3,4}$
Γ_1		π	σ
Γ_2	π		σ
$\Gamma_{3,4}$	σ	σ	π

Here, π and σ refer to the electric field of the laser radiation being parallel or perpendicular to the crystal axis, respectively. In these TSE experiments, the first laser frequency (Ω_1) was π polarized to match the transition from the $^7F_6$ (Γ_2) ground state to the lowest $^5D_4$ (Γ_1) intermediate state (see Figure 1). Then, the second laser frequency (Ω_2) was either π or σ polarized to allow for a transition to either a Γ_2 or a $\Gamma_{3,4}$ final state, respectively. The lowest $^5D_4$ (Γ_1) state is used as the intermediate step to ensure that no other intermediate states are populated.

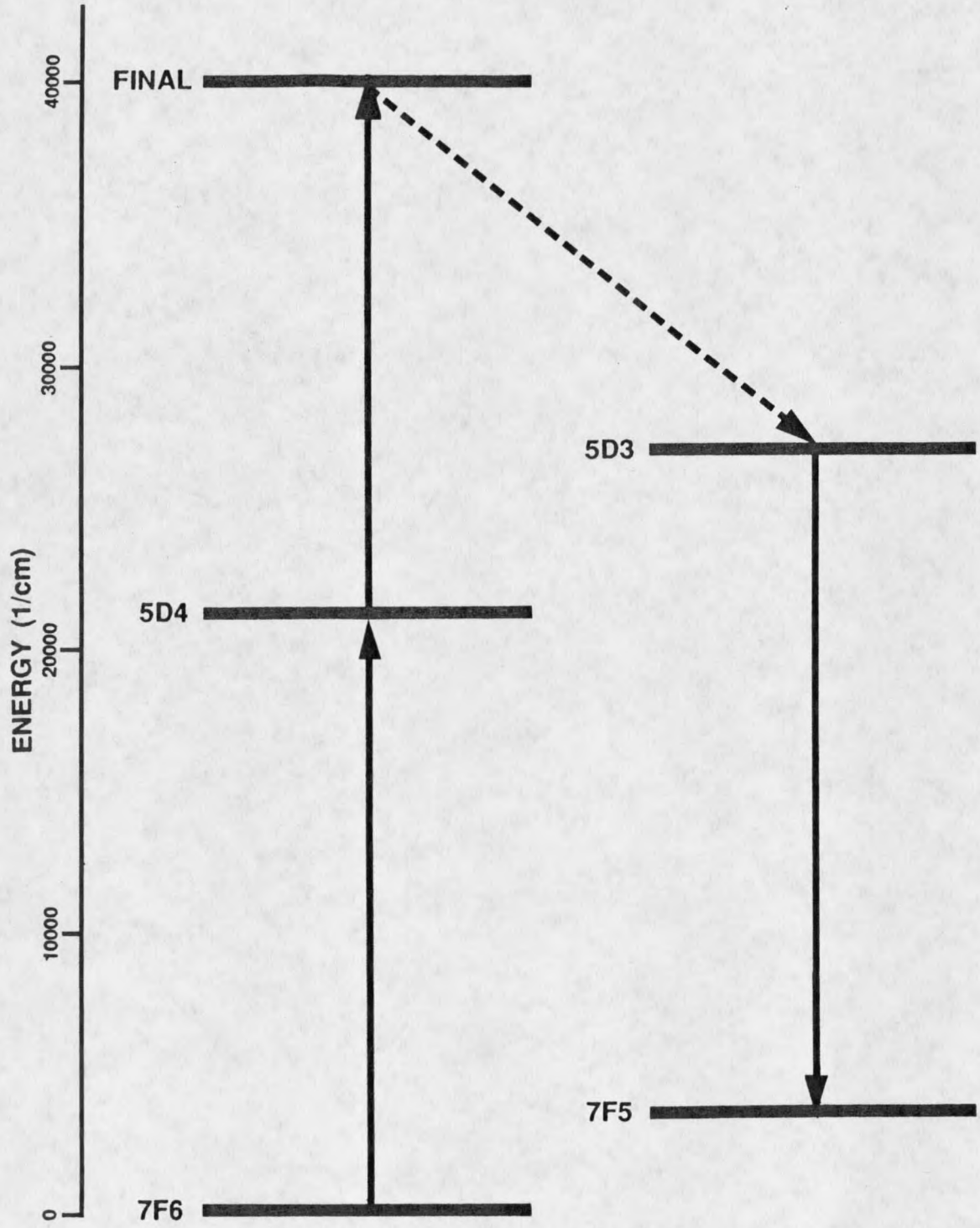

Figure 1. Partial energy level diagram of the Tb^{3+} ion for the two-step excitation experiments.

Since the $^5D_4$ intermediate state has a representation of Γ_1, the observation of Γ_1 final states is not allowed by TSE. This is where a complementary aspect of TPA comes in.

The selection rules for a TPA process are determined in much the same way as those of the single photon transitions.[24,25] In fact, they are identical to those of Raman scattering and are listed in Table 4 for a transition from a Γ_2 initial state.

Table 4. Selection rules for direct two-photon absorption

	Polarization with respect to the crystal axis		
	Γ_1	Γ_2	$\Gamma_{3,4}$
Γ_2	$\sigma\sigma,\pi\sigma,\sigma\pi$	$\pi\pi,\sigma\sigma,\pi\sigma,\sigma\pi$	$\pi\sigma,\sigma\pi$

In these direct two-photon transitions only one laser was used with an energy of $\hbar\Omega$. The transition would take place whenever $2\hbar\Omega$ matched the transition energy (see Figure 2). The labels $\pi\pi$ and $\sigma\sigma$ refer to the electric field of this one laser being parallel or perpendicular to the crystal axis. The labels $\pi\sigma$ and $\sigma\pi$ refer to the electric field being a linear combination of both polarizations. Using this last polarization configuration, the Γ_1 final states, as well as all the others, can be determined. It is a simple matter to classify the crystal field sublevels through a process of elimination.

Since two-photon transitions are very weak, it should be mentioned here how they were detected. Whenever a transition took place, the 410 nm anti-stokes ultraviolet fluorescence cascading from the $^5D_3$ state to the $^7F_5$ state could be observed (see Figures 1 and 2). This served as a very sensitive indicator of

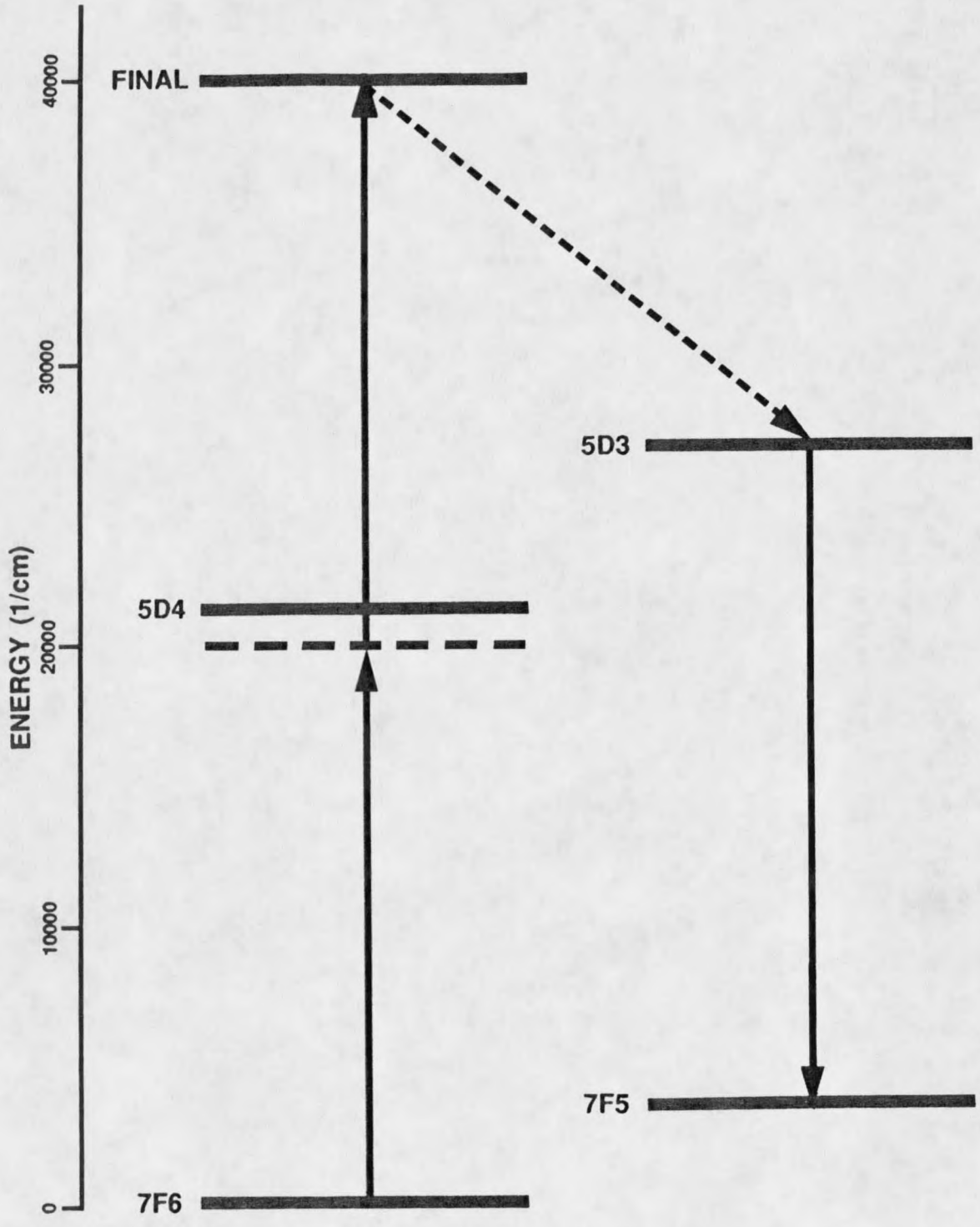

Figure 2. Partial energy level diagram of the Tb^{3+} ion for the direct two-photon absorption experiments.

the presence of a TPA transition. Experimental details will be described in the next chapter.

The selection rules determined via S_4 point group theory are by no means complete. One still has to consider the S, L, and J selection rules for the matrix elements in equation (2.8).

The initial, intermediate, and final states in equation (2.8) result from the odd terms of the crystal field operator, equation (2.13), admixing the original $4f^8$ states with those of the $4f^7 5d$ and $4f^7 5g$ configurations. This is the configuration mixing spoken of earlier. Then, through the Wigner-Eckart theorem [21] and the Judd-Ofelt approximation, we arrive at the selection rules

$$\Delta S = 0; \quad \Delta L \leq 6; \quad \Delta J \leq 6 \tag{2.16}$$

for single-photon transitons. For the direct two-photon transitions the operator within equation (2.11) is a second-rank tensor, giving rise through the Wigner-Eckart theorem to the selection rules for pure configurations as

$$\Delta S = 0; \quad \Delta L \leq 2; \quad \Delta J \leq 2. \tag{2.17}$$

Recent work concerning resonance enhancement may imply that these last symmetry rules could be broken as a result of mixed configurations. [9] Evidence to support this will be given in Chapter 4.

CHAPTER 3

EXPERIMENTAL ARRANGEMENT

Two experimental methods were utilized to determine the sublevels of the manifolds in question, these being direct two-photon absorption and two-step excitation. Both of these methods are complementary spectroscopic techniques as were described in Chapter 2. However, due to experimental difficulties which will be described in Chapter 4, the two-step excitation experiments were the primary means for gaining information on the majority of the manifolds in question.

In this chapter, these two experimental methods will be described in detail, along with the opto-galvanic calibration system used to calculate the energies and the computer control of the experiments.

Two-Photon Experiments

At the heart of the matter in any laser spectroscopy lab are the lasers themselves. Therefore, these will be described first before moving on to how they were utilized.

Lasers

Either one or two tunable dye lasers were used for these experiments, depending on which type of experiment was being done. For the direct two–photon

absorption experiments only one dye laser was used since the final excited state is created by the simultaneous absorption of two photons of the same energy coming from the same source. In the two-step excitation experiments two dye lasers were used. The first dye laser served to excite the atom from the ground state to a real intermediate state while the second laser was used to excite it from this real intermediate state to the final state.

The tunable dye lasers were based on a design conceived by T.W. Hänsch in 1972. [26] Each of these tunable dye lasers was pumped by its own pulsed nitrogen gas laser which operated at a wavelength of 337.1 nm, a pulse rate of 6 Hz and a pulse width of 10 nanoseconds. The timing between the two nitrogen gas lasers could be varied manually with a timing stabilization unit and was measured with a Tektronix 7912AD Programmable Digitizer. This was useful in later experiments when trying to determine the origins of certain ambiguous transitions, which will be discussed in detail in the next chapter. Both the tuneable dye lasers and the pulsed nitrogen gas lasers were constructed by Dr. R.L. Cone and his previous graduate students.

Typically, the nitrogen gas lasers were producing a power of 200-300 kW. Bearing in mind the pulse width of 10 nanoseconds, one realizes that the actual amount of energy in one pulse is on the order of only several millijoules. The beam, upon emerging from the nitrogen gas laser, is spatially rectangular with dimensions of roughly 1 cm in height and 2.5 cm in width. The bottom half of this beam was split off and sent to the oscillator section of the tunable dye laser while the top half of the beam continued on to the amplifier section of the dye laser. This pumping configuration was essentially the same for both dye lasers (see Figure 3).

Both dye lasers had an oscillator cavity defined by a partially reflecting

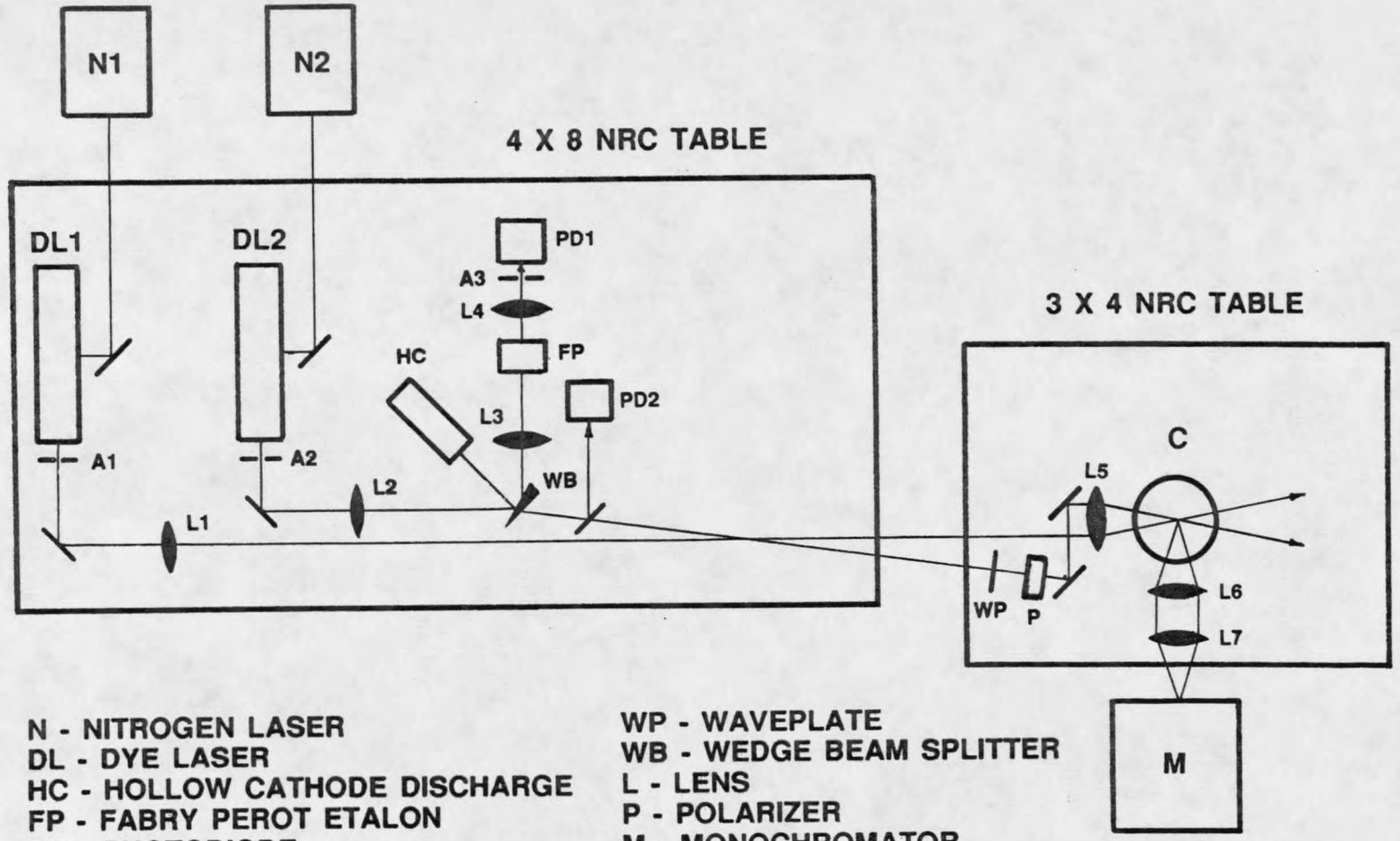

Figure 3. Experimental setup for the two-photon experiments

mirror at the front end and a 632 lines per millimeter reflection diffraction grating at the rear end. To fully illuminate the diffraction grating, a telescopic beam expander was inserted between the dye cell and the diffraction grating. The diffraction grating itself was mounted on a gimbal-type mount with micrometer adjustments for movement in both the vertical and horizontal planes. Motion in the horizontal plane would change the angle of the incident beam upon the grating, therefore changing the wavelength at which the dye laser would oscillate (within the constraints defined by the gain curve of the dye solution), while motion in the vertical plane would fine tune the lasing itself. It should be mentioned here that if the horizontal plane of rotation was not exactly parallel to the surface of the optics table the laser power would diminish considerably during a scan if not monitored. A spurious reflection from the main beam was monitored with a photodiode and oscilloscope, and periodically a vertical adjustment was made to the diffraction grating mount to maximize the laser power.

The dye solution was contained in cuvette-type dye cells. Motor driven magnetic stirrers maintained thermal homogeneity of the dye solution throughout the experiments. The dyes used in these experiments were Exciton 7D4TMC in a 10^{-2} molar solution of p-dioxane and Exciton Coumarin 500 in a 10^{-2} molar solution of ethanol. Both dye lasers were mounted on a Newport Research Corporation 4′ x 8′ optical table.

Direct Two-Photon Absorption Experiments

As was stated before, the direct two-photon absorption experiments required the use of only one tunable dye laser, specifically dye laser DL2 in Figure 3. The horizontal micrometer adjustment on the diffraction grating mount was attached to a stepper motor which was computer controlled. This way, the wavelength of the dye

laser could be changed at a continuous rate by moving the grating through a prescribed angle determined by the number of revolutions of the stepper motor. The output power of this laser was typically between 15-20 kW.

The beam, upon exiting the dye laser, continued on to a wedge beam splitter (WB) where two beams were split off to the calibration system (which will be described in a later section). This wedge beam splitter also refracted the beam so as to throw it slightly off the optic axis. The main part of the beam continued on to another beam splitter where a small part of the beam was monitored with a sample and hold photodiode (PD2) for recording the relative laser power. This laser power was later used for normalizing the fluorescence signal from the sample. The beam continued on to a $\lambda/2$ waveplate (WP) and a polarizer (P) so that the polarization of the incident radiation could be selected to be parallel ($\pi\pi$) or perpendicular ($\sigma\sigma$) to the crystal axis as well as a linear superposition of both these polarizations ($\pi\sigma/\sigma\pi$). A pair of 90° prism reflectors were used to bring the beam back on the optic axis and the beam was then focused onto the crystal with a 250 mm focal length lens, giving a minimum waist diameter of approximately 0.06 mm at the location of the crystal.

The crystal sat inside a glass cryostat (C) designed and built by Pope Scientific, Inc. which had optically transparent windows for the incoming laser beam as well as for observing the resulting UV fluorescence. The crystal was continuosly kept at pumped liquid helium temperatures ($T \approx 1.3$ K) for all of these experiments.

The fluorescence signal was collected by a 75 mm lens (L6) and focused onto the entrance slit of a MacPherson Model 218 f/5.3 monochromator (M) by a 200 mm focal length lens (L7). This monochromator was tilted 90° so that its entrance slit was parallel with the long path of the laser beam through the sample. This way, the maximum amount of fluorescence could be collected. A CS 5-58

glass bandpass filter was placed at the entrance slit of the monochromator to help filter out any reflected laser radiation and lower energy fluorescence from the $^5D_4$ level.

The UV fluorescence due to a direct two-photon absorption process was quite weak so a gated photon counting system was utilized for observing this signal (Figure 4) in order to eliminate the dark counts. An RCA C31034 photomultiplier tube (PMT) was mounted at the exit slit of the monochromator and was contained in a thermoelectric and water cooled housing manufactured by Pacific Precision Instruments. The PMT was operated at −1480 volts for the TPA experiments. The signal output from the PMT was fed into a preamplifier and then into a homemade discriminator and TTL pulse generator. These pulses were then gated to ensure that only those pulses coming from a fluorescence signal were passed. This gate was 3 milliseconds in duration with a delay of 5 microseconds. The remaining pulses were then counted by a Northern Scientific Model 575 Multichannel Analyzer. At the completion of each experiment these data were transferred to a PDP-11/03 microcomputer and later to a VAX 11/780 computer or VAX 8850 cluster for data analysis.

A brief word on alignment should be mentioned here before moving on. When the $^5D_4$ (Γ_1) state at 20553.5 cm^{-1} is populated, the resulting yellow fluorescence (18358.5 cm^{-1}) from this state to the ground state term $^7F_5$ is very strong and plainly visible with the naked eye from several meters away. The image of this fluorescence was easily placed on the monochromator entrance slit by the collection optics. The monochromator was then tuned to observe this yellow fluorescence and the signal from the PMT was fed directly into a Keithley Picoammeter. The needle deflection on the picoammeter thus gave a very accurate means of fine tuning the alignment of the beam and collection optics. Fortunately,

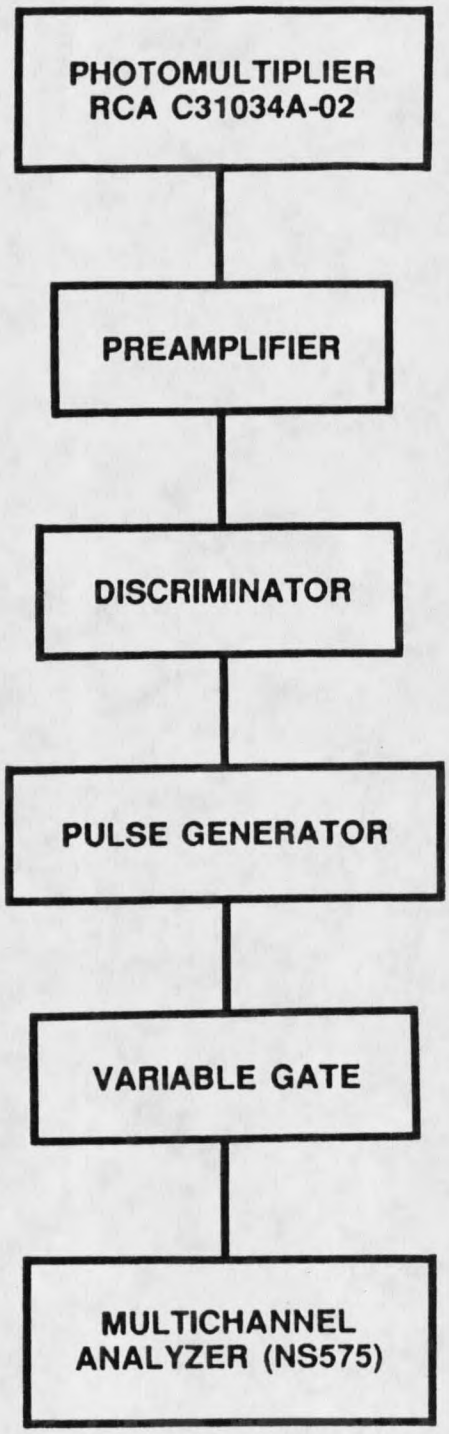

Figure 4. Photon counting system employed in the direct two-photon absorption experiments

the two laser dyes used both lased at 20553.5 cm^{-1} and this process of alignment could always be used. After the alignment was completed the monachromator was tuned back to observe the UV fluorescence, the CS 5-58 filter was reinserted, the laser was tuned to the starting energy of the scan, and the experiment was started.

Two-Step Excitation Experiments

These experiments required the use of both dye lasers DL1 and DL2 in Figure 3. Laser DL1, which will hereby be referred to as Ω_L, was tuned to match the the real intermediate $^5D_4$ state at 20553.5 cm^{-1}. This energy was held constant throughout these experiments. Laser DL2, which will hereby be referred to as Ω_H, was then scanned through an energy region in question. The UV anti-Stokes cascade fluorescence would then take place whenever $\Omega_L + \Omega_H$ resulted in a two-step transition.

The mechanics of this setup were almost identical to that of the direct two-photon absorption experiments, the only difference being the introduction of an additional dye laser. As stated before, this dye laser was pumped by its own pulsed nitrogen gas laser and the timing between the two lasers could be varied. The first set of two-step excitation experiments had Ω_H arriving after Ω_L on a time scale of the order of a microsecond, while the second set of experiments had Ω_H firing 0 to 5 nanoseconds after Ω_L. If Ω_H was set to fire before Ω_L the fluorescence signal would vanish. This served as a good test to see if the fluorescence signal was due to a two-step excitation process.

The laser powers were typically 5 to 10 kW for Ω_L and 15 to 20 kW for Ω_H. The polarization of Ω_L was left parallel to the crystal axis and the polarization of Ω_H was set either parallel ($\pi\pi$) or perpendicular ($\pi\sigma$) to the crystal axis.